PCCP

# A Molecular Beams and Computational Study on the Barrierless Gas Phase Formation of (Iso)Quinoline in Low Temperature Extraterrestrial Environments

| | |
|---|---|
| Journal: | *Physical Chemistry Chemical Physics* |
| Manuscript ID | CP-ART-05-2021-002169.R1 |
| Article Type: | Paper |
| Date Submitted by the Author: | 10-Jul-2021 |
| Complete List of Authors: | Zhao, Long; University of Hawaii at Manoa, Department of Chemistry<br>Prendergast, Matthew; University of Hawai'i at Manoa<br>Kaiser, Ralf; University of Hawaii,<br>Xu, Bo; Lawrence Berkeley National Laboratory, Chemical Sciences Division<br>Lu, Wenchao; Lawrence Berkeley National Laboratory, Chemical Sciences Division<br>Ahmed, Musahid; Lawrence Berkeley National Laboratory, Chemical Sciences Division<br>Howlader, A. Hasan; Florida International University, Department of Chemistry and Biochemistry<br>Wnuk, Stanislaw F.; Florida International University, Chemistry and Biochemistry<br>Korotchenko, Alexander; Samara National Research University<br>Evseev, Mikhail; Samara National Research University<br>Bashkirov, Eugene; Samara National Research University, General and Theoretical Physics<br>Azyazov, Valeriy; Samara National Research University; Lebedev Physical Institute of RAS, Department of Chemical & Electric Discharge Lasers<br>Mebel, Alexander; Florida International University, Chemistry and Biochemistry |
| | |

# A Molecular Beams and Computational Study on the Barrierless Gas Phase Formation of (Iso)Quinoline in Low Temperature Extraterrestrial Environments

Long Zhao, Matthew Prendergast, Ralf. I. Kaiser*
*Department of Chemistry, University of Hawaii at Manoa, Honolulu, HI 96822, USA*

Bo Xu, Wenchao Lu, Musahid Ahmed*
*Chemical Sciences Division, Lawrence Berkeley National Laboratory, Berkeley, CA 94720, USA*

A. Hasan Howlader, Stanislaw F. Wnuk*
*Department of Chemistry and Biochemistry, Florida International University, Miami, FL 33199, USA*

Alexander S. Korotchenko, Mikhail M. Evseev, Eugene K. Bashkirov
*Samara National Research University, Samara 443086, Russian Federation*

Valeriy N. Azyazov
*Lebedev Physical Institute, Samara 443011*
*and Samara National Research University, Samara 443086, Russian Federation*

Alexander M. Mebel*
*Department of Chemistry and Biochemistry, Florida International University, Miami, FL 33199, USA*

* Corresponding author:
Prof. Dr. Ralf I. Kaiser <ralfk@hawaii.edu>.
Dr. Musahid Ahmed <mahmed@lbl.gov>.
Prof. Dr. Stanislaw F. Wnuk <wnuk@fiu.edu>.
Prof. Dr. Alexander M. Mebel < mebela@fiu.edu>.

**ABSTRACT:** Despite remarkable progress toward the understanding of the formation pathways leading to polycyclic aromatic hydrocarbons (PAHs) in combustion systems and in deep space, the complex reaction pathways leading to nitrogen-substituted PAHs (NPAHs) at low temperatures of molecular clouds and hydrocarbon-rich, nitrogen-containing atmospheres of planets and their moons like Titan have remained largely obscure. Here, we demonstrate through laboratory experiments and computations that the simplest prototype of NPAHs - quinoline and isoquinoline ($C_9H_7N$) – can be synthesized via rapid and de-facto barrier-less reactions involving *o*-, *m*- and *p*-pyridinyl radicals ($C_5H_4N^{\bullet}$) with vinylacetylene ($C_4H_4$) under low-temperature conditions.

## 1. Introduction

During the last decade, significant progress has been made in untangling the fundamental elementary reactions leading to the gas phase formation of polycyclic aromatic hydrocarbons (PAHs) – organic molecules carrying fused benzene rings – with up to five six-membered rings through the exploitation of molecular beam experiments.[1-14] In deep space, PAH-like molecules have been suggested to account for up to 30% of the galactic carbon budget[15, 16] and provide decisive nucleation sites for the formation of carbonaceous dust particles.[17] From the spectroscopic viewpoint, PAH-like species have been also linked to the diffuse interstellar bands (DIBs) defined as discrete absorption features superimposed on the interstellar extinction curve ranging from the blue part of the visible (400 nm) to the near infrared (1.2 μm).[18] Further, PAHs and their cations, anions, radicals, and partially (de)hydrogenated counterparts are considered as carriers of the unidentified infrared (UIR) emission bands observed at 3.3, 6.2, 7.7, 11.2, and 12.7 μm;[19] these emissions likely result from ultraviolet pumped infrared fluorescence of PAHs with an excess of 50 carbon atoms.[19, 20] The identification of the simplest PAH naphthalene ($C_{10}H_8$) along with chemically more complex PAHs such as anthracene/phenanthrene ($C_{14}H_{10}$) and pyrene/fluoranthene ($C_{16}H_{10}$) in some 20 carbonaceous chondrites[21, 22] along with isotope (D, $^{13}C$) studies[23] infers their extraterrestrial origin in circumstellar envelopes of carbon-rich asymptotic giant branch (AGB) stars such as of IRC+10216 and possibly in planetary nebulae as their descendants. Overall, molecular beam experiments have revealed fundamental mass growth processes:[14, 24] i) Hydrogen Abstraction – Acetylene Addition (HACA),[3, 10] ii) Hydrogen Abstraction – Vinylacetylene Addition (HAVA),[2, 4, 5, 8] iii) Phenyl Addition – Dehydro-

Cyclization (PAC),[7] iv) Radical-Radical Reactions (RRR),[1] v) Methylidyne Addition - Cyclization – Aromatization (MACA),[25] vi) Hydrogen-Abstraction-Methyl-Addition,[26] vii) CHRCR,[27-29] and viii) aromatic α-alkynyl-linked hydrocarbon mechanism.[30] HAVA and MACA have no entrance barrier and are exoergic with all barriers involved ranging below the energy of the separated reactants. Consequently, these pathways have the capability to operate at low temperatures of cold molecular clouds such as TMC-1 and OMC-1 (10 K) and also in hydrocarbon rich atmospheres of planets and their moons like Titan and Pluto. These mechanistic concepts have provided a solid, experimentally and computationally verified framework to PAH formation in extreme environments from low temperatures settings to high temperature environments like circumstellar envelopes of carbon rich AGB stars and combustion systems at a few 1,000 K.

However, whereas well-defined routes to PAH formation have begun to emerge, surprisingly little is known about the synthesis of their nitrogen-substituted counterparts (NPAHs), which can be derived from PAHs by formally replacing one or more methylidyne (CH) moieties by isoelectronic nitrogen (N) atom(s). Parker et al. revealed that the reaction of pyridinyl radicals ($^{\bullet}C_5H_4N$) – isoelectronic reactants to the phenyl radical ($C_6H_5$) – with acetylene ($C_2H_2$) can lead at elevated temperatures to (iso)quinoline ($C_9H_7N$) via the classical Hydrogen Abstraction – Acetylene Addition (HACA) mechanism in analogy to the formation of naphthalene ($C_{10}H_8$) via HACA.[31] However, low temperature formation pathways to NPAHs are still obscure. This lack of knowledge is quite remarkable since the 6.2 μm UIR band could also originate from nitrogen-substituted gas phase PAHs.[32] Further, considering their molecular structures – PAHs have been contemplated as precursors to biorelevant molecules such as nucleobases – key building blocks in ribonucleic acid (RNA).[33, 34] The astrophysical relevance of nitrogen-substituted aromatic molecules is well documented since the discovery of biorelevant molecules such as vitamin B3 (niacin) and nucleobases (pyrimidines, purines) in carbonaceous chondrites like Murchison.[35-37] In particular, the detection of terrestrially unusual nucleobases, 6-diaminopurine and 6,8-diamino-purine in Murchison together with an $^{15}N/^{14}N$ isotope enrichment proposes an extraterrestrial source.[38, 39] Nevertheless, discrete formation mechanisms of NPAHs such as (iso)quinoline are unknown.

Here, we report the results of molecular beam experiments combined with electronic structure calculations on the reaction of three distinct pyridinyl radicals (*ortho*-, *meta*-, *para*-; *o*-, *m*-, *p*-; $^{\bullet}C_5H_4N$) with vinylacetylene ($H_2CCHCCH$; $C_4H_4$) (Figure 1). We reveal barrierless formation routes to (iso)quinolines ($C_9H_7N$) along with their substituted pyridine isomers in analogy to the Hydrogen Abstraction – Vinylacetylene Addition (HAVA) mechanisms leading to naphthalene ($C_{10}H_8$) in the isoelectronic phenyl – vinylacetylene system.[4] (Iso)quinoline can be formed via a single collision event of the *o*-, *m*-, or *p*-pyridinyl radical with vinylacetylene involving a van-der-Waals complex and a submerged barrier in the entrance channel. The facile route to (iso)quinoline in low temperature interstellar and Solar System gas phase environments such as in Saturn's moon Titan changes our perception how we think about the formation of NPAHs in deep space thus classifying cold molecular clouds like carbon-rich cores of TMC-1 and OMC-1 as potential molecular factories leading to NPAHs in low temperature interstellar environments.

## 2. Experimental

The experiments were conducted at the Advanced Light Source (ALS) at the Chemical Dynamics Beamline (9.0.2.) exploiting a high-temperature chemical reactor consisting of a resistively-heated silicon carbide (SiC) tube of 20 mm heating length and 1 mm inner diameter.[2, 40, 41] This device is situated inside the source chamber of a molecular beam apparatus equipped with a Wiley-McLaren reflectron time-of-flight mass spectrometer (Re-TOF-MS) and designed to study the outcome of elementary chemical reactions leading to PAH growth *in situ* through the reaction of aromatic radicals. In detail, iodinated pyridines ($C_5H_4NI$) [*o*-iodopyridine (> 98%, Sigma-Aldrich); *m*-, and *p*-iodopyridine (> 98%, TCI America)] were stored in separate experiments in a stainless-steel bubbler at 293 K. The radical reactants were generated *in situ* via pyrolysis of the iodinated precursors seeded in vinylacetylene/helium (5% $C_4H_4$, 95% He; Applied Gas) carrier gas at a reactor inlet pressure of 300 Torr. The temperature of the SiC tube was determined using a Type-C thermocouple to be 1,325 ± 10 K. At this temperature, each iodinated precursor dissociates to the corresponding radical plus atomic iodine *in situ* followed by the reaction of the aromatic radical with vinylacetylene (Figure 1). The molecular beam passed then through a 2 mm skimmer located 10 mm downstream the reactor and entered the main chamber, which houses the Re-TOF-MS. The products within the supersonic molecular

beam were then photoionized in the extraction region of the mass spectrometer by utilizing quasi-continuous tunable synchrotron vacuum ultraviolet (VUV) light. VUV single photon ionization represents essentially a fragment-free ionization technique and is dubbed as a *soft* ionization method compared to the harsher conditions of electron impact ionization leading often to excessive fragmentation of the parent ion.[28, 42] The ions formed via soft photoionization were extracted and introduced onto a microchannel plate detector through an ion lens. Under our experimental condition, the residence time in the reactor tube is few tens to hundreds of μs.[43] Control experiments were also conducted by expanding neat helium carrier gas with each iodinated precursor into the resistively-heated silicon carbide tube. No signal at *m/z* = 129 or 130, i.e. representing the molecular formula of ionized $C_9H_7N$ and $^{13}CC_8H_7N$, respectively, was observed in these control experiments. Finally, reference PIE curves of helium-seeded $C_4H_3$-substituted pyridines [2-(but-3-en-1-yn-1-yl)pyridine, (E)-2-(but-1-en-3-yn-1-yl)pyridine, 3-(but-3-en-1-yn-1-yl)pyridine, (E)-3-(but-1-en-3-yn-1-yl)pyridine, 4-(but-3-en-1-yn-1-yl)pyridine, (E)-4-(but-1-en-3-yn-1-yl)pyridine], quinoline ($C_9NH_7$), and isoquinoline ($C_9NH_7$) were recorded in the present work within the same experimental setup (Supplementary Information). These $C_4H_3$-branched pyridines were synthesized in house as described in the Supplementary Information; quinoline and isoquinoline were purchased from Millipore Sigma (99% +).

**3. Theoretical Methods**

The calculations of the energies and molecular parameters of various intermediates and transition states for the reactions of *o*-, *m*-, and *p*-pyridinyl with vinylacetylene on the $C_9NH_9$ potential energy surface (PES), as well as of the reactants and possible products were carried out at the G3(MP2,CC)//B3LYP/6-311G(d,p) level of theory. In particular, geometries were optimized and vibrational frequencies were calculated using the density functional B3LYP method[44, 45] with the 6-311G(d,p) basis set. Single-point total energies were subsequently refined via a series of coupled clusters CCSD(T) and second-order Møller-Plesset perturbation theory MP2 calculations, with the final energy computed as

E[G3(MP2,CC)] = E[CCSD(T)/6-311G(d,p)] + E[MP2/G3Large)] – E[MP2/6-311G(d,p)] + ZPE [B3LYP/6-311G(d,p)][46-48]

The G3(MP2,CC) model chemistry approach normally provides chemical accuracy of 0.01–0.02 Å for bond lengths, 1–2° for bond angles, and 3–6 kJ $mol^{-1}$ for relative energies of hydrocarbons,

their radicals, reaction energies, and barrier heights in terms of average absolute deviations.[47] For the entrance van der Waals complexes and ensuing transition states for a covalent bond formation between the $C_5NH_4$ radicals and $C_4H_4$, additional single point calculations were carried at the CCSD(T) level with Dunning's correlation-consistent basis sets cc-pVDZ and cc-pVTZ[49] with subsequent extrapolation to the complete basis set (CBS) limit[50] and at the explicitly correlated[51, 52] CCSD(T)-F12/cc-pVTZ-f12 level, which also aims to evaluate the CCSD(T)/CBS energy. Geometries and vibrational frequencies of the entrance van der Waals complexes and transition states were recalculated using the doubly-hybrid B2PLYPD3 density functional[53-55] with the same 6-311G(d,p) basis set. The single-point G3(MP2,CC), CCSD(T)/CBS, and CCSD(T)-F12/cc-pVTZ-f12 calculations were then repeated at the B2PLYPD3/6-311G(d,p)-optimized geometries. These additional calculations were carried out to evaluate the relative energies of the reactant complexes and entrance transition states with respect to the initial reactants, which are critical to determine feasibility of the $C_5NH_4 + C_4H_4$ reactions at extremely low temperatures. The calculations have shown that relative energies evaluated by the six different methods (B3LYP and B2PLYPD3 for geometries and zero-point vibrational energies (ZPE) and G3(MP2,CC), CCSD(T)/CBS, and CCSD(T)-F12/cc-pVTZ-f12 for single-point energies) agree within $\pm$2 kJ mol$^{-1}$. The GAUSSIAN 09[56] and MOLPRO 2010[57] program packages were employed for the ab initio calculations.

Product branching ratios in the $C_5NH_4 + C_4H_4$ reactions in the limit of zero pressure and extremely low temperature were evaluated through Rice-Ramsperger-Kassel-Marcus (RRKM) calculations[58-60] of unimolecar rate constants for the reaction steps beginning with the **oi1**, **mi1**, **pi1** intermediates produced in the entrance channels. Here, the rate constants were evaluated as functions of the available internal energy of each intermediate or transition state within the harmonic approximation using B3LYP/6-311G(d,p) frequencies, with the internal energy assumed to be equal to the chemical activation energy, that is, negative of the relative energy of a species with respect to the reactants, which corresponds to a zero collision energy. Only one energy level was considered throughout as at a zero-pressure limit emulating the conditions in cold molecular clouds. RRKM rate constants were used to compute product branching ratios by solving first-order kinetic equations within steady-state approximation.[61]

## 4. Results and Discussion

### 4.1.1. Experimental Results - Mass Spectrometric Result

Once formed in the high-temperature microreactor, the products were probed in a supersonic molecular beam coupled to synchrotron-based mass spectrometry through photoionization. Representative mass spectra recorded at 9.50 eV for the reactions of *o*-, *m*- and *p*-pyridinyl radicals with vinylacetylene along with the data of the control experiments of pyrolyzed, helium-seeded iodopyridine precursors *without* vinylacetylene are presented in Figure 2. It is evident that signal at *m/z* = 129 and 130 is *only* observable in the reaction systems (Figures 2a, 2c and 2e) of the pyridinyl radicals with vinylacetylene, but not in the control experiments *without* vinylacetylene (Figures 2b, 2d and 2f). Ion counts at *m/z* = 78, 79, 205, 206 and 254 were detectable in *both* the reaction systems and in the control experiments; this finding indicates that these species are not formed from reaction of pyridinyl radicals with vinylacetylene. The mass spectra alone deliver compelling evidence that the products at *m/z* = 129 and 130 are the consequence of the reactions of pyridinyl radical (78 amu) with vinylacetylene (52 amu) followed by atomic hydrogen loss. Signal at *m/z* = 205 and 206 can be linked to the precursors ($C_5H_4NI$) and their $^{13}$C-counterparts ($^{13}CC_4H_4NI$). The thermal dissociation of the precursors leads to pyridinyl radicals ($C_5H_4N^{\bullet}$) observed at *m/z* = 78. Signal at *m/z* = 79 represents a combination of ion counts from $^{13}$C-substituted pyridinyl radicals and pyridine ($C_5H_5N$); the latter is formed via hydrogen atom addition to pyridinyl radicals. It is noticeable that iodine ($I_2$) molecules (*m/z* = 254) are also formed, most likely through recombination of two iodine atoms.

### 4.1.2. Experimental Results - Photoionization Efficiency Spectra

Having identified signal at *m/z* = 129 and 130 as the outcome of reactions between pyridinyl radicals with vinylacetylene (Figures 1 and 2), we are attempting now to identify the nature of the structural isomer(s) formed. This is achieved by extracting the photoionization efficiency curves (PIE); these curves report the ion intensity of a well-defined mass-to-charge ratio as a function of the photon energy. By fitting the experimental PIE curves at well-defined m/z ratios with the linear combination of known, reference PIE curves, we can then identify the molecule(s) contributing to the ion counts at distinct m/z ratios, i.e. *m/z* = 129 and 130. Here, the PIE graphs were collected over the photon energy range from 8.00 to 10.00 eV in steps of 0.05 eV (Figure 3). It is important to note that the experimental PIE profiles of *m/z* = 129 and 130 are superimposable after rescaling for each system; this indicates that signal at *m/z* = 130 is associated with the $^{13}$C-counterparts of *m/z* = 129 ($C_9H_7N^+$). In detail, a linear combination of

recorded reference PIE curves of distinct $C_9H_7N$ isomers could replicate the experimental PIE curves for each system (Figure 3).

**First**, in the *o*-pyridinyl - vinylacetylene system, the PIE curve of *m/z* = 129 reveals a clear onset at 8.45 ± 0.05 eV (Figure 3a); this onset corresponds to the adiabatic ionization energy (IE) of (E)-2-(but-1-en-3-yn-1-yl)pyridine (8.45 ± 0.05 eV; **P3**) (Figure 4). However, this isomer cannot alone replicate the experimentally recorded PIE curve. The overall fit reveals that a linear combination of the PIE curves of quinoline (**P1**), (E)-2-(but-1-en-3-yn-1-yl)pyridine (**P3**), and 2-(but-3-en-1-yn-1-yl)pyridine (**P4**), could replicate the experimental data. The ion counts of the three isomers have a branching ratio of **P1** : **P3** : **P4** of 19.6 ± 2.0% : 70.3 ± 7.0% : 10.1 ± 1.0% at the photon energy of 10.00 eV. It should be noticed that these percentage values do not represent the branching ratios of the individual isomer; the latter cannot be determined since their photoionization cross sections are unknown and hence not available. **Second**, in the *m*-pyridinyl - vinylacetylene system (Figs. 3c and 3d), the onset at 8.50 ± 0.05 eV corresponds to the IE of (E)-3-(but-1-en-3-yn-1-yl)pyridine (8.50 ± 0.05 eV; **P5**). The overall fit could be achieved with a combination of four reference $C_9H_7N$ PIE curves: quinoline (**P1**), isoquinoline (**P2**), (E)-3-(but-1-en-3-yn-1-yl)pyridine (**P5**), and 3-(but-3-en-1-yn-1-yl)pyridine (**P6**). The branching ratio of the ion counts of these four isomers **P1** : **P2** : **P5** : **P6** was determined to be 7.8 ± 0.8% : 7.9 ± 0.8% : 75.8 ± 7.6% : 2.5 ± 0.3% at 10.00 eV. **Finally**, in the *p*-pyridinyl - vinylacetylene system (Figs. 3e and 3f), the onset agrees with the adiabatic IE of isoquinoline (8.55 ± 0.05 eV; **P2**). The measured PIE curve at m/z =129 could be fit with isoquinoline (**P2**), (E)-4-(but-1-en-3-yn-1-yl)pyridine (**P7**), and 4-(but-3-en-1-yn-1-yl)pyridine (**P8**) with ratios of the ion counts for **P2** : **P7** : **P8** of 23.7 ± 2.4% : 66.1 ± 6.7% : 10.2 ± 1.0% at 10.00 eV.

Overall, the reactions of *o*-, *m*- and *p*-pyridinyl with vinylacetylene reveal the formation of bicyclic reaction products (quinoline, isoquinoline) along with but-3-en-1-yn-1-yl- and (E)-but-1-en-3-yn-1-yl-substituted pyridines at the *o*-, *m*- and *p*-positions, respectively (Figure 4). Quinoline is formed in the *o*- and *m*-pyridinyl - vinylacetylene systems, while isoquinoline is detected in the *m*- and *p*-pyridinyl - vinylacetylene systems. The reference PIE curves for both quinoline and isoquinoline are different both in the onset of photoionization signal (ionization energy) and their shapes (Figure S4).

### 4.2 Theoretical Results

We are now merging the experimental results with electronic structure calculations in an attempt to unravel the reaction mechanisms. PES profiles for the reactions of pyridinyl radicals with vinylacetylene, where the latter adds to the radical site by its vinylic end, operational even at very low temperatures are exhibited in Figures 5a to 5c for *o*-, *m*-, and *p*-pyridinyl, respectively. The surfaces corresponding to $C_4H_4$ addition by the $C_2H$ group are provided in the Supplementary Information (Figures S5).

### 4.2.1 *o*-Pyridinyl - Vinylacetylene System

Let us first focus on the reaction mechanism in the *o*-pyridinyl - vinylacetylene system (Figures 5a and S5a). The vinylacetylene molecule approaches the *o*-pyridinyl radical forming a weakly stabilized (-10 kJ $mol^{-1}$) van-der Waals complex **oi0**. This complex isomerizes via addition of the radical center of the *o*-pyridinyl radical to the $CH_2$ moiety of the vinylacetylene molecule forming a nitrogen-containing resonantly stabilized doublet radical intermediate **oi1**. As computed at the G3(MP2,CC)//B3LYP/6-311G(d,p) + ZPE level of theory, this addition requires overcoming a barrier of 9 kJ $mol^{-1}$ meaning that the energy of the transition state is 1 kJ $mol^{-1}$ below the total energy of the separated reactants, hence, a submerged barrier. At the CCSD(T)/CBS and CCSD(T)-F12/cc-pVTZ-f12 levels of theory, the position of the transition state is close to +1 kJ $mol^{-1}$, which indicates that, considering the anticipated error bars of the calculations, the addition proceeds either without or with a very low activation energy. The intermediate **oi1** can decompose via atomic hydrogen loss to (E)-2-(but-1-en-3-yn-1-yl)pyridine (**P3**). Alternatively, an isomerization sequence via a hydrogen shift from the aromatic ring to the C2 atom of the chain moiety (**oi2**), cyclization (**oi3**), and a hydrogen shift to the carbene moiety to **oi4** is terminated by an atomic hydrogen loss followed by aromatization to form the bicyclic quinoline (**P1**). It should be noted that, besides the entrance transition state whose relative energy could be slightly positive but close to zero, all intermediates and transition states of this reaction sequence are located below the energy of the separated reactants; therefore, the reactions to form **P1** and **P3** are actually barrierless or nearly barrierless.

Apart from these two products observed in *o*-pyridinyl - vinylacetylene system, a third product 2-(but-3-en-1-yn-1-yl)pyridine (**P4**) was also detected. The PES (Figure S5a) indicates that the van-der Waals structure **oi0** can isomerize via addition of the *o*-pyridinyl to the terminal

CH moiety of vinylacetylene yielding intermediate **oi5**; the transition state involved is higher than the energy of the separated reactants. A hydrogen atom loss from the acetylenic group of the vinylacetylene chain leads to the formation of 2-(but-3-en-1-yn-1-yl)pyridine (**P4**) in an overall exoergic reaction (-11 kJ $mol^{-1}$). However, the exit transition state resides 8 kJ $mol^{-1}$ above the separated products. This barrier can be easily overcome in the high temperature conditions of the reactor, but it cannot be passed in cold environments such as in molecular clouds (10 K).

Alternatively, **oi5** can isomerize to **oi7** via hydrogen atom migration from the aromatic ring to the C2 atom of the side chain. Successive hydrogen migrations drive **oi7** to **oi8** and **oi9**, from C1 in the sidechain back to C3 on the ring and from C4 to C1 at the $C_4H_4$ moiety, respectively. Hydrogen atom loss from **oi9** yields the product (E)-2-(but-1-en-3-yn-1-yl)pyridine (**P3**). In an alternative pathway, **oi9** isomerizes to an exotic bicyclic structure with a six and a four-membered-ring intermediate **oi10**, which then ring-opens to **oi11** thus achieving a conformational change from *trans* in **oi9** to *cis* in **oi11**; the latter isomerized through ring-closure to **oi12**, which contains the quinoline backbone. This intermediate eventually loses a hydrogen atom to yield quinoline (**P1**). Alternatively, starting from **oi7**, a cyclization process leads to the formation of **oi13**, which then ring opens to **oi14**; here again, the four-member ring closure and opening change the conformation of the side chain from *trans* in **oi7** to *cis* in **oi14**. Intermediate **oi15** - produced via the ring-closure of **oi14** – can eject atomic hydrogen to form quinoline (**P1**). Finally, hydrogen shifts dictate the sequence from **oi14** to **oi16**, which *cis-trans* isomerizes to **oi17**. Hydrogen atom losses convert **oi16** and **oi17** to (Z)-2-(but-1-en-3-yn-1-yl)pyridine (**P9**) and (E)-2-(but-1-en-3-yn-1-yl)pyridine (**P3**), respectively.

### 4.2.2 *m*-Pyridinyl - Vinylacetylene System

Similar to the mechanisms in the *o*-pyridinyl - vinylacetylene system, the vinylacetylene molecule approaches the *m*-pyridinyl radical forming a weakly stabilized (-8 kJ $mol^{-1}$) van-der Waals complex **mi0** (Figures 5b and S5b). The complex isomerizes to intermediate **mi1** via addition of the radical center in m-pyridinyl to the $CH_2$ moiety of vinylacetylene through a small barrier of 5 kJ $mol^{-1}$. Once again, the barrier to addition is below the energy of the separated reactants and hence can be classified as a submerged barrier. Moreover, in this case CCSD(T)/CBS and CCSD(T)-F12 levels of theory confirm that the energy of the transition state is negative relative to the reactants. A hydrogen atom loss from **mi1** leads to the experimentally

detected product (E)-3-(but-1-en-3-yn-1-yl)pyridine (**P5**). Alternatively, the reaction sequence **mi1** → **mi2** → **mi3** → **mi4** → **P1** involving a hydrogen shift from the aromatic ring to the C2 atom in the chain, cyclization, a hydrogen migration in the aromatic moiety to the carbene, and hydrogen atom elimination leading eventually to the formation of quinoline (**P1**). A second pathway via **mi1** → **mi5** → **mi6** → **mi7** → **P2**, effectively converts **mi1** to isoquinoline (**P2**) along with a hydrogen atom. All barriers involved in these reaction pathways are below the separated reactants. Note that from **mi1**, quinoline formation is suggested to proceed favorable compared to isoquinoline considering the lower barriers for hydrogen migrations (to **mi2** versus **mi5**) and ring closure (to **mi3** versus **mi6**).

Besides quinoline (**P1**), isoquinoline (**P2**) and (E)-3-(but-1-en-3-yn-1-yl)pyridine (**P5**), 3-(but-3-en-1-yn-1-yl)pyridine (**P6**) is also a detected product in the *m*-pyridinyl - vinylacetylene experiment. As we will demonstrate below, pathways to this product require overcoming transition states located above the energy of the separated reactants. In detail, **P6** can be formed via hydrogen atom loss from intermediate **mi8**, which is generated via isomerization of **mi0** through the addition of the radical center in *m*-pyridinyl to the terminal acetylenic moiety of $C_4H_4$ molecule. This reaction pathway requires overcoming a barrier of only 3 kJ mol$^{-1}$ higher than the separated reactants; this process can happen under the high-temperature condition in our experiments, but not in cold molecular clouds. Intermediate **mi8** may also undergo isomerization to **mi10** and/or and **mi17** via distinct hydrogen shifts. These intermediates eventually yield through multi-step isomerization pathways to quinoline (**P1**), isoquinoline (**P2**), (E)-3-(but-1-en-3-yn-1-yl)pyridine (**P5**), (Z)-3-(but-1-en-3-yn-1-yl)pyridine (**P10**), and 3-(but-3-en-1-yn-1-yl)pyridine (**P6**). Finally, **mi9** is generated via addition of the *m*-pyridinyl radical to the CH vinylenic carbon atom of vinylacetylene by overcoming a barrier of 13 kJ mol$^{-1}$ relative to the reactants. The subsequent reaction sequences may lead to quinoline (**P1**), isoquinoline (**P2**), and (E)-3-(but-1-en-3-yn-1-yl)pyridine (**P5**). Overall, unlike the sole detection and formation of the NPAH quinoline in the *o*-pyridinyl - vinylacetylene system, two NPAHs (quinoline, isoquinoline) are formed in the *m*-pyridinyl system since **mi1** can undergo hydrogen migration from the ortho and para carbon atom of the pyridine moiety to the C2 carbon of the vinylacetylene chain.

### 4.2.3 *p*-Pyridinyl - Vinylacetylene System

As presented in Figure 5c, the PES for the *p*-pyridinyl - vinylacetylene reaction system for the $C_4H_4$ addition by its vinylic end has similar features of the *o*-pyridinyl - vinylacetylene system leading eventually to the formation of isoquinoline (**P2**) and (E)-4-(but-1-en-3-yn-1-yl)pyridine (**P7**). The key difference between these two systems is that the addition via the submerged barrier leads eventually to the formation of isoquinoline (**P2**) instead of quinoline (**P1**), owing to the discrepancy between the location of the radical centers in the *ortho*- and *para*-positions of pyridinyl radicals. It should be also noted that the CCSD(T)/CBS and CCSD(T)-F12 calculations for the *p*-pyridinyl plus vinylacetylene system corroborate negative energy of the entrance transition state with respect to the reactants and hence a submerged character of the reaction barrier. The third experimentally observed product 4-(but-3-en-1-yn-1-yl)pyridine (**P8**) is formed in analogy to 2-(but-3-en-1-yn-1-yl)pyridine (**P4**) and 3-(but-3-en-1-yn-1-yl)pyridine (**P6**) via hydrogen atom loss of intermediate **pi6**; this intermediate is generated from the isomerization of the van-der Waals complex **pi0** via addition of *p*-pyridinyl to the CH group of vinylacetylene. High energy pathways have to overcome barriers, which are not accessible in cold molecular clouds (Figure S5c).

## 5. Conclusions

Our study provides compelling evidence on the de-facto barrierless formation of two NPAHs isovalent to naphthalene ($C_{10}H_8$) - quinoline ($C_9H_7N$, **P1**) and isoquinoline ($C_9H_7N$, **P2**) - in cold molecular clouds in overall exoergic reactions. In all three systems, the reactions are initiated by the formation of a van-der-Waals complex (**oi0, mi0, pi0**) stabilized by 8 to 23 kJ $mol^{-1}$ with respect to the separated reactants. These complexes then isomerize via addition of the carbon-centered radicals to the $CH_2$ moiety of vinylacetylene via barriers lower than the energy of the separated reactants (submerged barriers) leading to resonantly stabilized doublet radical inter-mediates (**oi1, mi1, pi1**). While a submerged character of the entrance transition states is consistently confirmed by different levels of theoretical calculations in the *m*- and *p*-pyridinyl – vinylacetylene reaction systems, for *o*-pyridinyl the barrier might be slightly positive, but it is close to zero within the expected error bars of the present calculations. Each of the initially formed radical intermediates can evolve through essentially two reaction pathways. Pathway one is dictated by a hydrogen atom loss from the $CH_2$ moiety of vinylacetylene leading in weakly endoergic reactions (-13 to – 34 kJ $mol^{-1}$) to *o*-, *m*-, and *p*-$C_4H_3$ substituted pyridines: 2, 3, and 4-(but-1-en-3-yn-1-yl)pyridines (**P3, P5, P7**). Alternatively, **oi1, mi1, pi1** eventually form

quinoline ($C_9H_7N$, **P1**) and isoquinoline ($C_9H_7N$, **P2**) via three isomerization steps through hydrogen shifts from the pyridine moiety to the C2 atom of the side chain, cyclization, hydrogen shift in the annulated ring moiety to the carbene carbon atom terminated by hydrogen atom loss and aromatization in overall exoergic reactions. These pathways follow identical features as the Hydrogen Abstraction – Vinylacetylene Addition (HAVA) mechanism[2, 4, 5, 8] leading to the isovalent naphthalene ($C_{10}H_8$) molecule through barrierless ring annulation of the phenyl radical – the isoelectronic species of *o*-, *m*-, and *p*-pyridinyl). Comparing the pathways of both NPAHs to PAH formation, the replacement of the CH moiety in the phenyl reactant by a nitrogen atom effectively destabilizes the reaction intermediates and transition states on the inherent PESs by about 20 kJ mol$^{-1}$. However, the apparent facile concept of isoelectronicity, which predicts analogous reaction pathways to naphthalene and (iso)quinoline based on the $C_6H_5$-$C_4H_4$ and $C_5H_4N$-$C_4H_4$ and hence the replacement of a CH moiety by a nitrogen atom in the aromatic reactant cannot be expanded to the vinylacetylene reactant. The replacement of a CH moiety by a nitrogen leads to vinyl cyanide ($C_2H_3CN$). The isovalent $C_6H_5$-$C_2H_3CN$ system was shown not to form (iso)quinolone under conditions of cold molecular clouds. Here, in strong discrepancy to the $C_5H_4N$-$C_4H_4$ systems, the nitrogen atom does not act as a spectator, but is actively engaged in the chemistry in the $C_6H_5$-$C_2H_3CN$ system through the formation of a carbon-hydrogen bond. The involvement of the nitrogen atom in the reaction dynamics and the stability of the cyano group results in energetically unfavorable transition states located at least 13 kJmol$^{-1}$ above the separated reactants thus effectively blocking this pathway in cold molecular clouds, and also in the experiments.[62] Based on the PESs relevant to conditions in cold molecular clouds (Figures 5a-c), we also conducted statistical calculations to predict the relative branching ratios of the (but-1-en-3-yn-1-yl)pyridines versus the NPAHs (quinoline, isoquinoline). At the zero-pressure and zero-temperature limit, the RRKM calculations reveal overwhelming formation of the NPAHs: 99.7% of quinoline to 0.3% of **P3** for *o*-pyridinyl plus $C_4H_4$, 98.9% of isoquinoline to 1.1% of **P7** for *p*-pyridinyl, and 94.4% of quinolone and 5.5% of isoquinoline to 0.1% of **P5** for *m*-pyridinyl. However, higher temperatures increase the relative yields of the (but-1-en-3-yn-1-yl)pyridines **P1**, **P3**, and **P5** due to entropic preference of their formation channels.

Note that besides the aforementioned products, the present studies also identified three (but-3-en-1-yn-1-yl) pyridine products (**P4, P6, P8**), which can be formally derived by replacing the terminal carbon atom of the acetylenic functional group in vinylacetylene by distinct pyridinyl

groups. In molecular clouds, however, pathways to these isomers are blocked since that the addition of the pyridinyl radicals to the terminal carbon atom of the acetylenic moiety has entrance barriers above the energy of the separated reactants (Figures S5a-c). However, these barriers can be overcome under the high temperature conditions in our chemical reactor.

To summarize, the present work provides a facile conceptual framework on the barrierless, low temperature formation of two prototypes of NPAHs - quinoline ($C_9H_7N$, **P1**) and isoquinoline ($C_9H_7N$, **P2**) – in the gas phase of cold molecular clouds in analogy to the Hydrogen Abstraction – Vinylacetylene Addition (HAVA) mechanism.[2, 4, 5, 8] Low temperature conditions also hold for hydrocarbon-rich atmospheres of planets, their moons (Titan),[63] and trans-Neptunian Objects (TNOs) such as Pluto,[64] where solar photons initiate a vigorous low temperature photochemistry of their methane – nitrogen based atmospheres. The pathways derived here require the presence of pyridine ($C_5H_5N$), which can be photolyzed to *o*-, *m*-, and *p*-pyridinyl radicals ($C_5H_4N$), and vinylacetylene ($C_4H_4$), which was recently observed in the cold molecular cloud TMC-1,[65] but not (yet) in Titan's or Pluto's atmosphere (Figure 6). However, both in the interstellar medium and in Pluto's and Titan's atmospheres, the ethylene ($C_2H_4$) and ethynyl ($C_2H$) reactants can easily form vinylacetylene as demonstrated by Zhang et al.[66] Three barrierless and exoergic pathways have been derived to form pyridine: i) reaction of 1,3-butadiene ($C_4H_6$) with cyano (CN) radicals (albeit with yields of a fraction of a percent at most),[67, 68] ii) reaction of vinylcyanide ($C_2H_3CN$) with cyano vinyl (HCCHCN),[31] and iii) reactions of methylidyne (CH) radicals with pyrrole ($C_4H_5N$).[69] Therefore, the aforementioned 'ingredients' – with the exception of pyrrole – suggest that pyridine, quinoline, and isoquinoline should form in cold molecular clouds as well as in Titan's and Pluto's atmosphere. However, the detectability of (iso)quinoline by microwave spectroscopy on these environments critically depends on the actual fractional abundance, which are dictates not only by their formation, but also destruction pathways such as by photodissociation[70-72] and fast chemical reactions such as with ground state carbon atoms.[73]

**Acknowledgements**

This work was supported by the US Department of Energy, Basic Energy Sciences DE-FG02-03ER15411 (experimental studies) and DE-FG02-04ER15570 (computational studies), to the University of Hawaii and to Florida International University. M. A. is supported by the Director,

Office of Science, Office of Basic Energy Sciences, of the U.S. Department of Energy under Contract No. DE-AC02-05CH11231, through the Gas Phase Chemical Physics Program, Chemical Sciences Division. The Advanced Light Source is supported by the same contract. Theoretical calculations at Lebedev Physics Institute were supported by the Ministry of Higher Education and Science of the Russian Federation by the grant No. 075-15-2021-597.

## Author contributions

R.I.K. directed the overall project. A.H.H synthesized the molecular calibration chemicals; L.Z., M.P, B.X. and W.L. carried out the experimental measurements; L.Z. performed the data analysis; A.S.K., M.M.E., E.K.B. V.N.A. and A.M.M. carried out the theoretical analysis; ALL the authors discussed the data. R.I.K., M.A. and A.M.M. supervised the project. S.F.W. supervised the synthesis processes. L.Z., R.I.K. and A.M.M. wrote the manuscript.

## Competing financial interests

The authors declare no competing financial interests.

## References

1. L. Zhao, R. I. Kaiser, W. Lu, B. Xu, M. Ahmed, A. N. Morozov, A. M. Mebel, A. H. Howlader and S. F. Wnuk, *Nat. Commun.*, 2019, **10**, 1-7.
2. L. Zhao, R. I. Kaiser, B. Xu, U. Ablikim, M. Ahmed, M. M. Evseev, E. K. Bashkirov, V. N. Azyazov and A. M. Mebel, *Nat. Astron.*, 2018, **2**, 973.
3. L. Zhao, R. I. Kaiser, B. Xu, U. Ablikim, M. Ahmed, D. Joshi, G. Veber, F. R. Fischer and A. M. Mebel, *Nat. Astron.*, 2018, **2**, 413-419.
4. L. Zhao, R. I. Kaiser, B. Xu, U. Ablikim, M. Ahmed, M. V. Zagidullin, V. N. Azyazov, A. H. Howlader, S. F. Wnuk and A. M. Mebel, *J. Phys. Chem. Lett.*, 2018, **9**, 2620-2626.
5. L. Zhao, R. I. Kaiser, B. Xu, U. Ablikim, W. Lu, M. Ahmed, M. M. Evseev, E. K. Bashkirov, V. N. Azyazov, M. V. Zagidullin, A. N. Morozov, A. H. Howlader, S. F. Wnuk, A. M. Mebel, D. Joshi, G. Veber and F. R. Fischer, *Nat. Commun.*, 2019, **10**, 1510.
6. L. Zhao, M. Prendergast, R. I. Kaiser, B. Xu, U. Ablikim, W. Lu, M. Ahmed, A. D. Oleinikov, V. N. Azyazov and A. H. Howlader, *Phys. Chem. Chem. Phys.*, 2019, **21**, 16737-16750.
7. L. Zhao, M. B. Prendergast, R. I. Kaiser, B. Xu, U. Ablikim, M. Ahmed, B. J. Sun, Y. L. Chen, A. H. Chang and R. K. Mohamed, *Angew. Chem.-Int. Ed.*, 2019, **58**, 17442-17450.
8. L. Zhao, B. Xu, U. Ablikim, W. Lu, M. Ahmed, M. M. Evseev, E. K. Bashkirov, V. N. Azyazov, A. H. Howlader and S. F. Wnuk, *ChemPhysChem*, 2019, **20**, 791-797.
9. L. Zhao, S. Doddipatla, R. I. Kaiser, W. Lu, O. Kostko, M. Ahmed, L. B. Tuli, A. N. Morozov, A. H. Howlader and S. F. Wnuk, *Phys. Chem. Chem. Phys.*, 2021, **23**, 5740-5749.
10. D. S. Parker, R. I. Kaiser, T. P. Troy and M. Ahmed, *Angew. Chem.-Int. Ed.*, 2014, **53**, 7740-7744.
11. M. Baroncelli, Q. Mao, S. Galle, N. Hansen and H. Pitsch, *Phys. Chem. Chem. Phys.*, 2020, **22**, 4699-4714.

12. D. S. Parker, F. Zhang, Y. S. Kim, R. I. Kaiser, A. Landera, V. V. Kislov, A. M. Mebel and A. Tielens, *Proc. Nat. Acad. Sci. U.S.A.*, 2012, **109**, 53-58.
13. D. D. S. Parker, D. F. Zhang, D. R. I. Kaiser, D. V. V. Kislov and D. A. M. Mebel, *Chem. Asian J.*, 2011, **6**, 3035-3047.
14. R. I. Kaiser and N. Hansen, *J. Phys. Chem. A*, 2021, **125**, 3826-3840.
15. P. Ehrenfreund and M. A. Sephton, *Faraday Discuss.*, 2006, **133**, 277-288.
16. E. Herbst and E. F. van Dishoeck, *Annu. Rev. Astron. Astrophys.*, 2009, **47**, 427-480.
17. W. W. Duley, *Astrophys. J.*, 2000, **528**, 841-848.
18. A. M. Ricks, G. E. Douberly and M. A. Duncan, *Astrophys. J.*, 2009, **702**, 301-306.
19. A. G. G. M. Tielens, *Annu. Rev. Astron. Astrophys.*, 2008, **46**, 289-337.
20. J. Puget and A. Léger, *Annu. Rev. Astron. Astrophys.*, 1989, **27**, 161-198.
21. R. Zenobi, J. M. Philippoz, R. N. Zare, M. R. Wing, J. L. Bada and K. Marti, *Geochim Cosmochim Acta*, 1992, **56**, 2899-2905.
22. H. Naraoka, A. Shimoyama and K. Harada, *Mineral. Mag.*, 1998, **62A**, 1056-1057.
23. H. Naraoka, A. Shimoyama and K. Harada, *Earth Planet. Sci. Lett.*, 2000, **184**, 1-7.
24. A. M. Mebel, A. Landera and R. I. Kaiser, *J. Phys. Chem. A*, 2017, **121**, 901-926.
25. C. He, A. A. Nikolayev, L. Zhao, A. M. Thomas, S. Doddipatla, G. R. Galimova, V. N. Azyazov, A. M. Mebel and R. I. Kaiser, *J. Phys. Chem. A*, 2021, **125**, 126-138.
26. N. Hansen, M. Schenk, K. Moshammer and K. Kohse-Höinghaus, *Combust. Flame*, 2017, **180**, 250-261.
27. K. Johansson, M. Head-Gordon, P. Schrader, K. Wilson and H. Michelsen, *Science*, 2018, **361**, 997-1000.
28. H. Jin, L. Xing, D. Liu, J. Hao, J. Yang and A. Farooq, *Combust. Flame*, 2021, **225**, 524-534.
29. J. D. Savee, T. M. Selby, O. Welz, C. A. Taatjes and D. L. Osborn, *J. Phys. Chem. Lett.*, 2015, **6**, 4153-4158.
30. P. Liu, H. Jin, B. Chen, J. Yang, Z. Li, A. Bennett, A. Farooq, S. M. Sarathy and W. L. Roberts, *Fuel*, 2021, **295**, 120580.
31. D. S. N. Parker, R. I. Kaiser, O. Kostko, T. P. Troy, M. Ahmed, B.-J. Sun, S.-H. Chen and A. H. H. Chang, *Phys. Chem. Chem. Phys.*, 2015, **17**, 32000-32008.
32. D. M. Hudgins, C. W. Bauschlicher Jr and L. J. Allamandola, *Astrophys. J.*, 2005, **632**, 316.
33. Z. Peeters, O. Botta, S. B. Charnley, R. Ruiterkamp and P. Ehrenfreund, *Astrophys. J.*, 2003, **593**, L129-L132.
34. M. P. Kroonblawd, R. K. Lindsey and N. Goldman, *Chem. Sci.*, 2019, **10**, 6091-6098.
35. K. E. Smith, M. P. Callahan, P. A. Gerakines, J. P. Dworkin and C. H. House, *Geochimica et Cosmochimica Acta*, 2014, **136**, 1-12.
36. M. P. Callahan, K. E. Smith, H. J. Cleaves, J. Ruzicka, J. C. Stern, D. P. Glavin, C. H. House and J. P. Dworkin, *Proc. Nat. Acad. Sci. U.S.A.*, 2011, **108**, 13995-13998.
37. Z. Martins, O. Botta, M. L. Fogel, M. A. Sephton, D. P. Glavin, J. S. Watson, J. P. Dworkin, A. W. Schwartz and P. Ehrenfreund, *Earth Planet. Sci. Lett.*, 2008, **270**, 130-136.
38. R. K. Robins, *J. Amer. Chem. Soc.*, 1958, **80**, 6671-6679.
39. S. Pizzarello and W. Holmes, *Geochimica et Cosmochimica Acta*, 2009, **73**, 2150-2162.
40. D. S. N. Parker, R. I. Kaiser, B. Bandyopadhyay, O. Kostko, T. P. Troy and M. Ahmed, *Angew. Chem.-Int. Ed.*, 2015, **54**, 5421-5424.
41. T. Yang, R. I. Kaiser, T. P. Troy, B. Xu, O. Kostko, M. Ahmed, A. M. Mebel, M. V. Zagidullin and V. N. Azyazov, *Angew. Chem.-Int. Edit.*, 2017, **56**, 4515-4519.
42. F. Qi, *Proc. Combust. Inst.*, 2013, **34**, 33-63.
43. M. V. Zagidullin, R. I. Kaiser, D. Porfiriev, I. P. Zavershinskiy, M. Ahmed, V. N. Azyazov and A. M. Mebel, *J. Phys. Chem. A*, 2018, **122**, 8819-8827.
44. A. D. Becke, *J. Chem. Phys.*, 1993, **98**, 5648-5652.
45. C. Lee, W. Yang and R. G. Parr, *Phys. Rev. B: Condens. Matter*, 1988, **37**, 785-789.

46. L. A. Curtiss, K. Raghavachari, P. C. Redfern, V. Rassolov and J. A. Pople, *J. Chem. Phys.*, 1998, **109**, 7764-7776.
47. L. A. Curtiss, K. Raghavachari, P. C. Redfern, A. G. Baboul and J. A. Pople, *Chem. Phys. Lett.*, 1999, **314**, 101-107.
48. A. G. Baboul, L. A. Curtiss, P. C. Redfern and K. Raghavachari, *J. Chem. Phys.*, 1999, **110**, 7650-7657.
49. T. H. Dunning Jr, *J. Chem. Phys.*, 1989, **90**, 1007-1023.
50. J. M. Martin and O. Uzan, *Chem. Phys. Lett.*, 1998, **282**, 16-24.
51. G. Knizia, T. B. Adler and H.-J. Werner, *J. Chem. Phys.*, 2009, **130**, 054104.
52. T. B. Adler, G. Knizia and H.-J. Werner, *J. Chem. Phys.*, 2007, **127**, 221106.
53. S. Grimme, *J. Chem. Phys.*, 2006, **124**, 034108.
54. L. Goerigk and S. Grimme, *J. Chem. Theory Comput.*, 2011, **7**, 291-309.
55. S. Grimme, S. Ehrlich and L. Goerigk, *J. Comput. Chem.*, 2011, **32**, 1456-1465.
56. M. J. Frisch, G. W. Trucks, H. B. Schlegel, G. E. Scuseria, M. A. Robb, J. R. Cheeseman, G. Scalmani, V. Barone, B. Mennucci, G. A. Petersson, H. Nakatsuji, M. Caricato, X. Li, H. P. Hratchian, A. F. Izmaylov, J. Bloino, G. Zheng, J. L. Sonnenberg, M. Hada, M. Ehara, K. Toyota, R. Fukuda, J. Hasegawa, M. Ishida, T. Nakajima, Y. Honda, O. Kitao, H. Nakai, T. Vreven, J. A. Montgomery, Jr., J. E. Peralta, F. Ogliaro, M. Bearpark, J. J. Heyd, E. Brothers, K. N. Kudin, V. N. Staroverov, T. Keith, R. Kobayashi, J. Normand, K. Raghavachari, A. Rendell, J. C. Burant, S. S. Iyengar, J. Tomasi, M. Cossi, N. Rega, J. M. Millam, M. Klene, J. E. Knox, J. B. Cross, V. Bakken, C. Adamo, J. Jaramillo, R. Gomperts, R. E. Stratmann, O. Yazyev, A. J. Austin, R. Cammi, C. Pomelli, J. W. Ochterski, R. L. Martin, K. Morokuma, V. G. Zakrzewski, G. A. Voth, P. Salvador, J. J. Dannenberg, S. Dapprich, A. D. Daniels, O. Farkas, J. B. Foresman, J. V. Ortiz, J. Cioslowski and D. J. Fox, *Gaussian 09, revision A.02*, 2009, **(Gaussian Inc., CT)**.
57. H. J. Werner, P. J. Knowles, G. Knizia, F. R. Manby, M. Schütz, P. Celani, W. Györffy, D. Kats, T. Korona, R. Lindh, A. Mitrushenkov, G. Rauhut, K. R. Shamasundar, T. B. Adler, R. D. Amos, A. Bernhardsson, A. Berning, D. L. Cooper, M. J. O. Deegan, A. J. Dobbyn, F. Eckert, E. Goll, C. Hampel, A. Hesselmann, G. Hetzer, T. Hrenar, G. Jansen, C. Köppl, Y. Liu, A. W. Lloyd, R. A. Mata, A. J. May, S. J. McNicholas, W. Meyer, M. E. Mura, A. Nicklaß, D. P. O'Neill, P. Palmieri, D. Peng, K. Pflüger, R. Pitzer, M. Reiher, T. Shiozaki, H. Stoll, A. J. Stone, R. Tarroni, T. Thorsteinsson and M. Wang, *MOLPRO, version 2010.1,* http://www.molpro.net, 2010, **(University College Cardiff Consultants Ltd, United Kingdom)**.
58. P. J. Robinson and K. A. Holbrook, *Unimolecular reactions*, Wiley: New York, 1972.
59. H. Eyring and S. H. Lin, *Basic chemical kinetics*, John Wiley & Sons, Inc., 1980.
60. J. I. Steinfeld, J. S. Francisco and W. L. Hase, *Chemical kinetics and dynamics*, Prentice Hall Upper Saddle River, NJ, 1999.
61. V. Kislov, T. Nguyen, A. Mebel, S. Lin and S. Smith, *J. Chem. Phys.*, 2004, **120**, 7008-7017.
62. J. Bouwman, A. Bodi and P. Hemberger, *Phys. Chem. Chem. Phys.*, 2018, **20**, 29910-29917.
63. R. M. C. Lopes, S. D. Wall, C. Elachi, S. P. D. Birch, P. Corlies, A. Coustenis, A. G. Hayes, J. D. Hofgartner, M. A. Janssen, R. L. Kirk, A. LeGall, R. D. Lorenz, J. I. Lunine, M. J. Malaska, M. Mastroguiseppe, G. Mitri, C. D. Neish, C. Notarnicola, F. Paganelli, P. Paillou, V. Poggiali, J. Radebaugh, S. Rodriguez, A. Schoenfeld, J. M. Soderblom, A. Solomonidou, E. R. Stofan, B. W. Stiles, F. Tosi, E. P. Turtle, R. D. West, C. A. Wood, H. A. Zebker, J. W. Barnes, D. Casarano, P. Encrenaz, T. Farr, C. Grima, D. Hemingway, O. Karatekin, A. Lucas, K. L. Mitchell, G. Ori, R. Orosei, P. Ries, D. Riccio, L. A. Soderblom and Z. Zhang, *Space Sci. Rev.*, 2019, **215**, 33.
64. M. Scherf, H. Lammer, N. V. Erkaev, K. E. Mandt, S. E. Thaller and B. Marty, *Space Sci. Rev.*, 2020, **216**, 123.
65. K. L. Kelvin Lee, R. A. Loomis, A. M. Burkhardt, I. R. Cooke, C. Xue, M. A. Siebert, C. N. Shingledecker, A. Remijan, S. B. Charnley, M. C. McCarthy and B. A. McGuire, *Astrophys. J.*, 2021, **908**, L11.
66. F. Zhang, P. Maksyutenko and R. I. Kaiser, *Phys. Chem. Chem. Phys.*, 2012, **14**, 529-537.

67. B. Sun, C. Huang, S. Chen, S. Chen, R. Kaiser and A. Chang, *J. Phys. Chem. A*, 2014, **118**, 7715-7724.
68. S. B. Morales, C. J. Bennett, S. D. Le Picard, A. Canosa, I. R. Sims, B. Sun, P. Chen, A. H. Chang, V. V. Kislov and A. M. Mebel, *Astrophys. J.*, 2011, **742**, 26.
69. S. Soorkia, C. A. Taatjes, D. L. Osborn, T. M. Selby, A. J. Trevitt, K. R. Wilson and S. R. Leone, *Phys. Chem. Chem. Phys.*, 2010, **12**, 8750-8758.
70. R. McCarroll, *AIP Conf. Proc.*, 2004, **740**, 3-19.
71. M. F. Lin, Y. A. Dyakov, C. M. Tseng, A. M. Mebel, S. H. Lin, Y. T. Lee and C. K. Ni, *J. Chem. Phys.*, 2005, **123**, 054309.
72. K. A. Prather and Y. T. Lee, *Isr. J. Chem.*, 1994, **34**, 43-53.
73. M. Lucas, A. M. Thomas, R. I. Kaiser, E. K. Bashkirov, V. N. Azyazov and A. M. Mebel, *J. Phys. Chem. A*, 2018, **122**, 3128-3139.

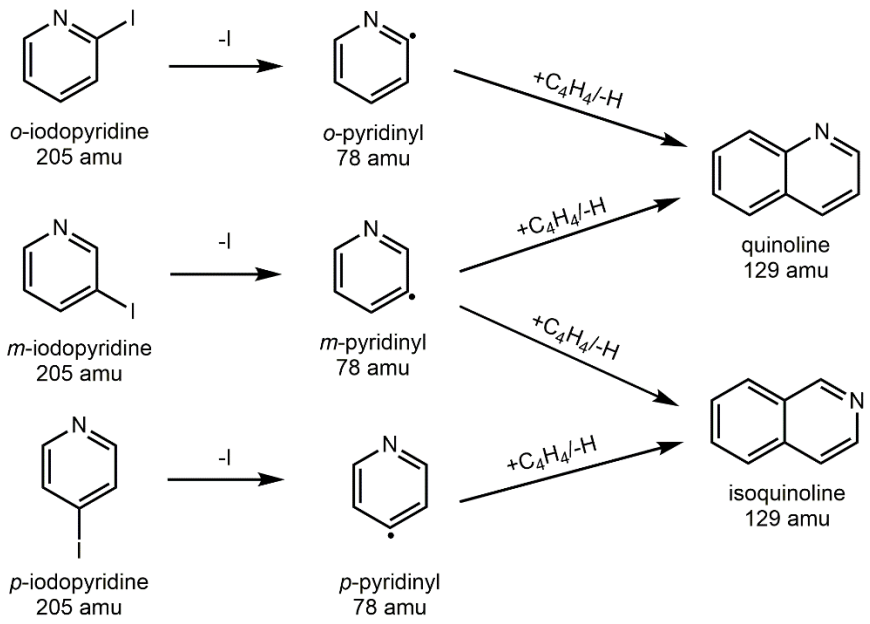


**Figure 1**. Schematic representation of the formation of quinoline ($C_9H_7N$) and isoquinoline ($C_9H_7N$) from the reaction of *o*-, *m*- and *p*-pyridinyl radicals ($C_5H_4N^{\bullet}$) with vinylacetylene ($C_4H_4$). *o*-, *m*- and *p*-pyridinyl radicals are produced from the pyrolysis of corresponding precursors, which are *o*-, *m*- and *p*-iodopyridines ($C_5H_4NI$), respectively.

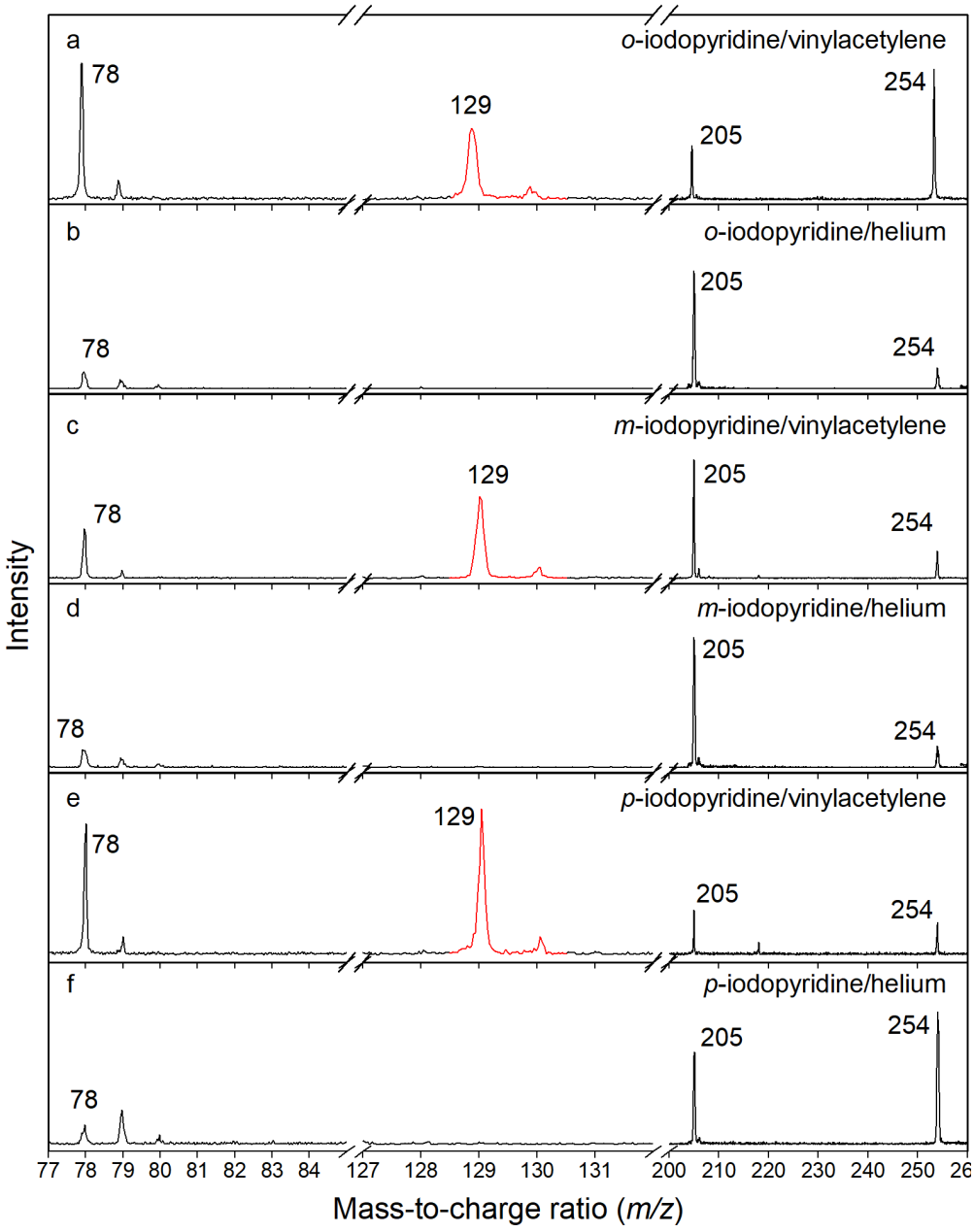


**Figure 2**. Comparison of photoionization mass spectra recorded at a photon energy of 9.50 eV. (a) *o*-iodopyridine ($C_5H_4NI$) - vinylacetylene ($C_4H_4$) system; (b) *o*-iodopyridine ($C_5H_4NI$) - helium (He) system; (c) *m*-iodopyridine ($C_5H_4NI$) - vinylacetylene ($C_4H_4$) system; (d) *m*-iodopyridine ($C_5H_4NI$) - helium (He) system; (e) *p*-iodopyridine ($C_5H_4NI$) - vinylacetylene ($C_4H_4$) system; and (f) *p*-iodopyridine ($C_5H_4NI$) - helium (He) system. The mass peaks of the newly formed species of interest along with the $^{13}C$-counterparts are highlighted in red.

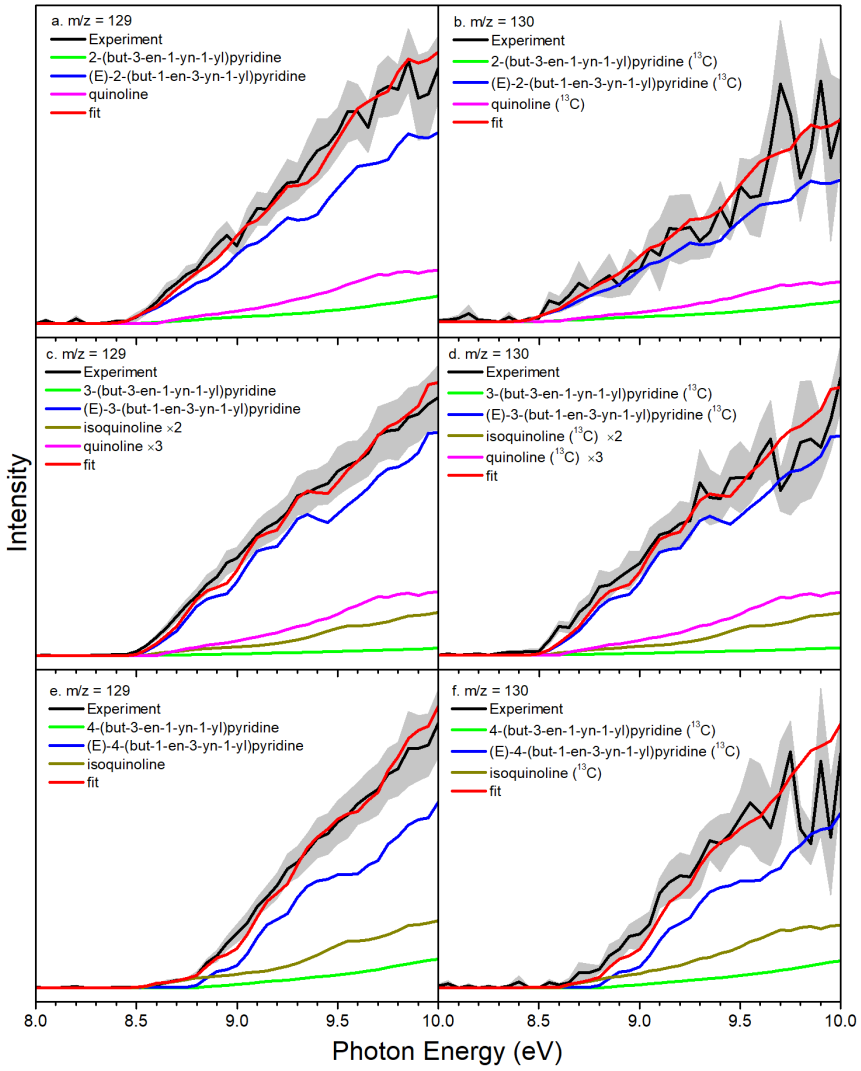


**Figure 3.** Photoionization efficiency (PIE) curves of *m/z* = 129 and 130 for reactions *o*-pyridinyl - vinylacetylene (a and b), *m*-pyridinyl - vinylacetylene (c and d), and *p*-pyridinyl/ vinylacetylene (e and f). Black: experimentally derived PIE curves; colored lines (green, blue, dark yellow and purple): reference PIE curves; red lines: overall fit. The overall error bars consist of two parts: ±10% based on the accuracy of the photodiode and a 1 σ error of the PIE curve averaged over the individual scans.

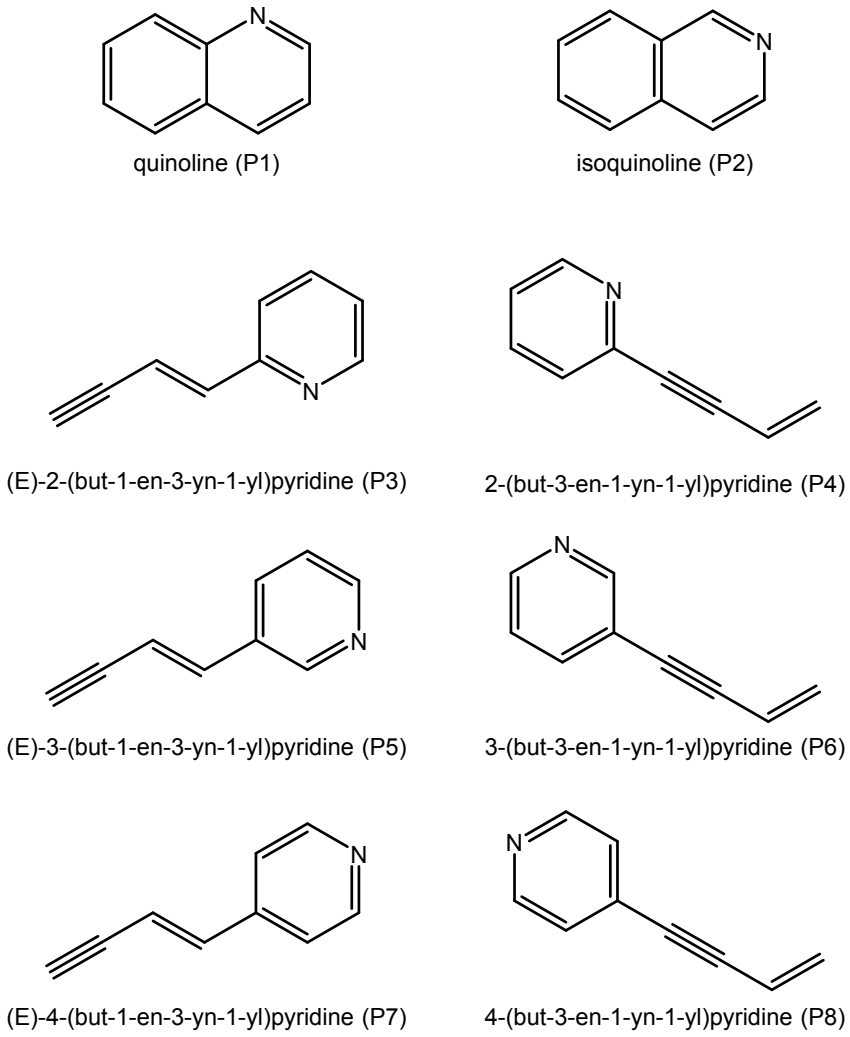


**Figure 4**. The molecular structures of the products observed in this work.

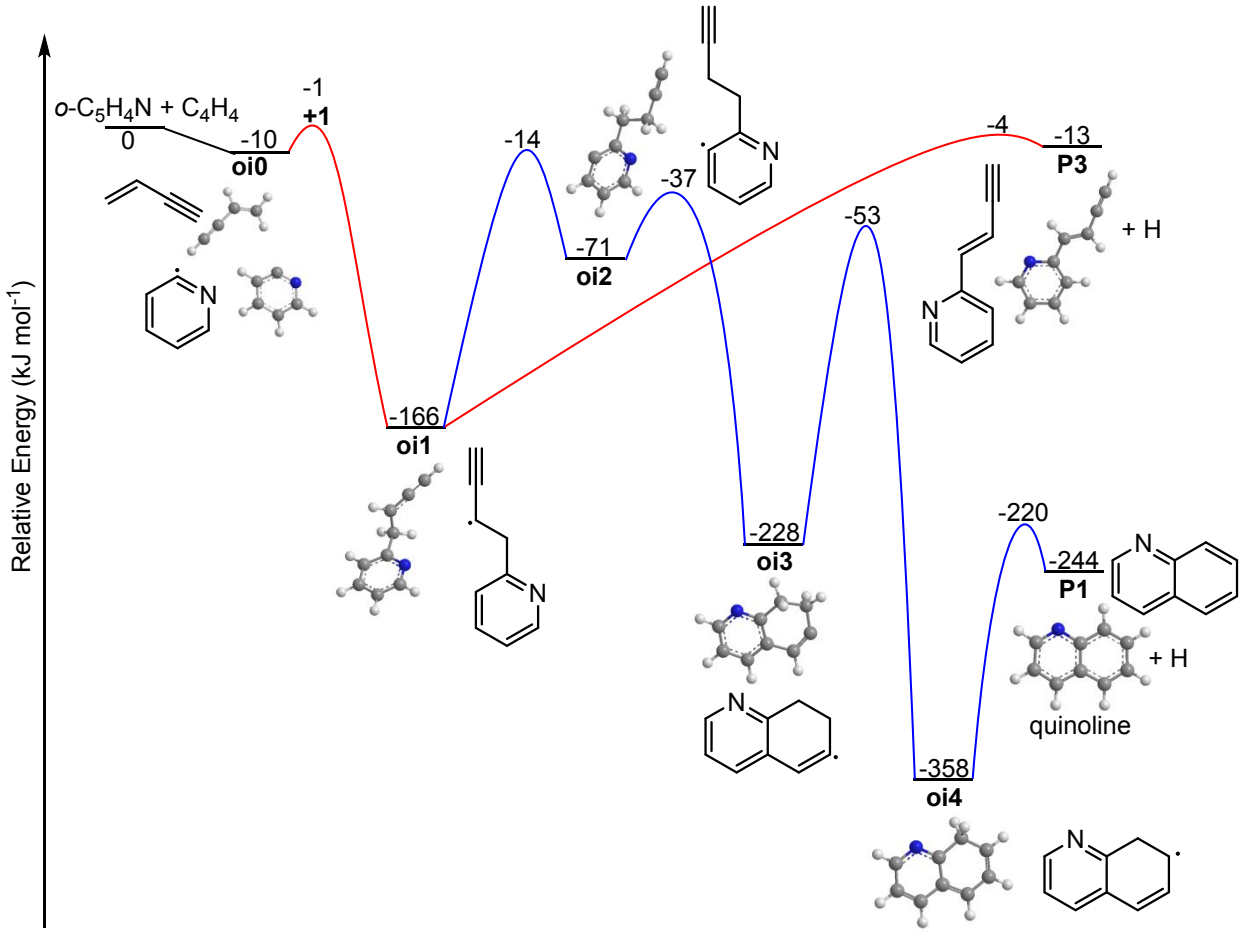


**Figure 5a.** Computed potential Energy Surface (PES) for the reaction system of *o*-pyridinyl ($C_5H_4N^{\bullet}$) and vinylacetylene ($C_4H_4$). The energies calculated at the G3(MP2,CC)//B3LYP/6-311G(d,p) + ZPE level of theory are presented in units of kJ $mol^{-1}$. The bold number shows the relative energy of the **oi0-oi1** transition state calculated at the CCSD(T)-F12/cc-pVTZ-f12//B3LYP/6-311G(d,p) + ZPE level. Only pathways open under conditions in cold molecular clouds are shown. For a surface describing the addition by the acetylenic end of $C_4H_4$, please confer to Figure S5a.

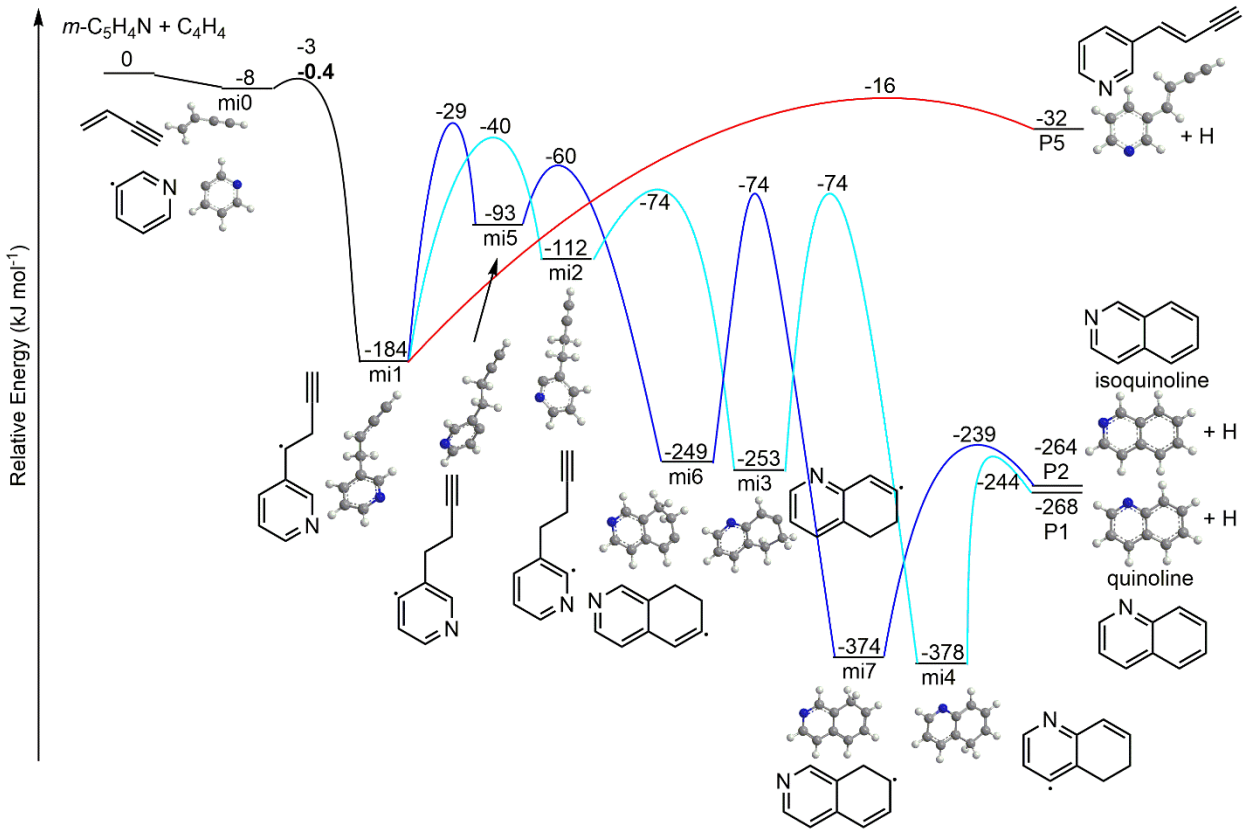


**Figure 5b.** Computed potential Energy Surface (PES) for the reaction system of *m*-pyridinyl ($C_5H_4N^{\bullet}$) and vinylacetylene ($C_4H_4$). The energies calculated at the G3(MP2,CC)//B3LYP/6-311G(d,p) + ZPE level of theory are presented in units of kJ $mol^{-1}$. The bold number shows the relative energy of the **mi0-mi1** transition state calculated at the CCSD(T)-F12/cc-pVTZ-f12//B3LYP/6-311G(d,p) + ZPE level. Only pathways open under conditions in cold molecular clouds are shown. For a surface describing the addition by the acetylenic end of $C_4H_4$, please confer to Figure S5b.

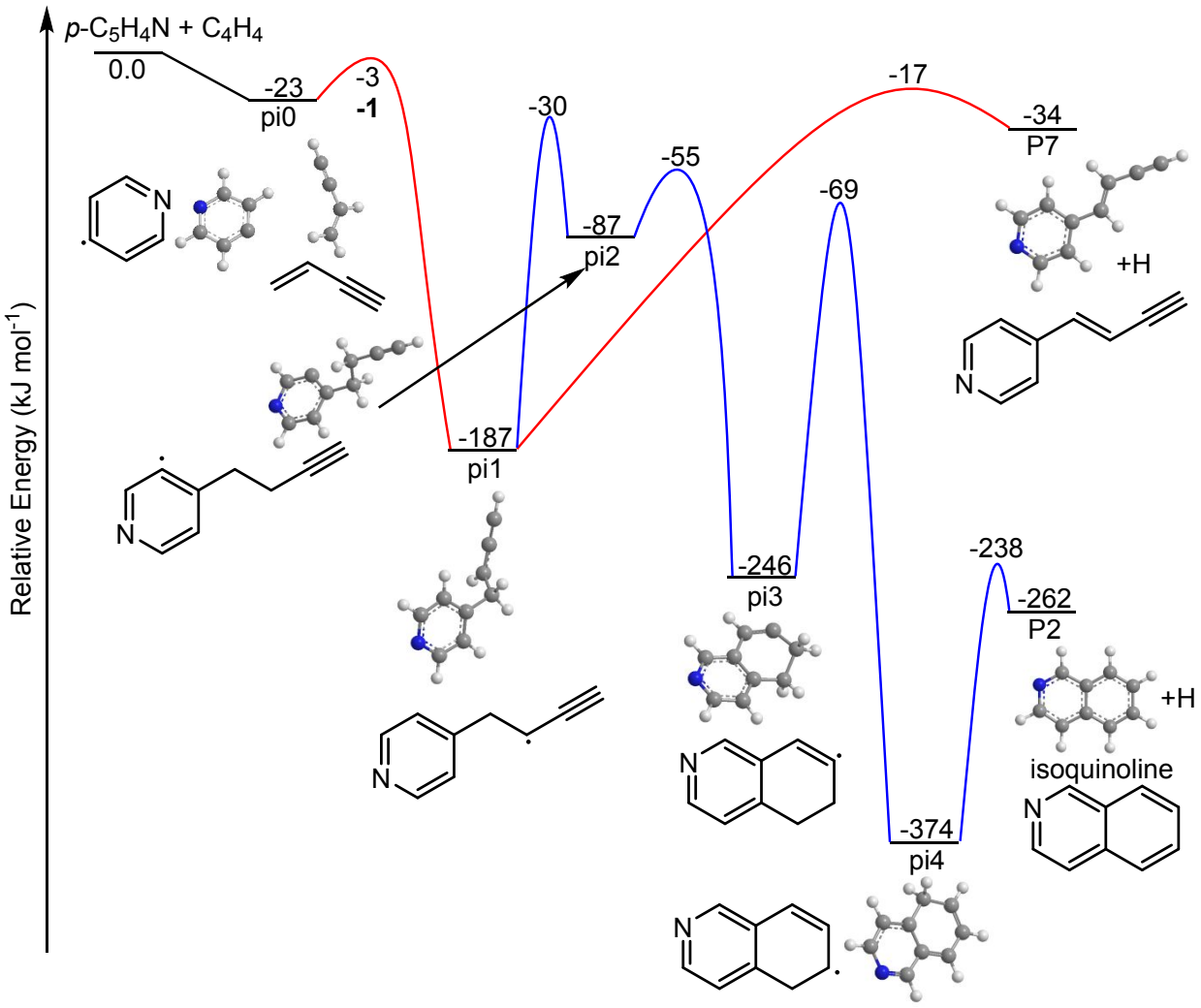


**Figure 5c.** Computed potential Energy Surface (PES) for the reaction system of *p*-pyridinyl ($C_5H_4N^{\bullet}$) and vinylacetylene ($C_4H_4$). The energies calculated at the G3(MP2,CC)//B3LYP/6-311G(d,p) + ZPE level of theory are presented in units of kJ mol$^{-1}$. The bold number shows the relative energy of the **pi0-pi1** transition state calculated at the CCSD(T)-F12/cc-pVTZ-f12//B3LYP/6-311G(d,p) + ZPE level. Only pathways open under conditions in cold molecular clouds are shown. For a surface describing the addition by the acetylenic end of $C_4H_4$, please confer to Figure S5c.

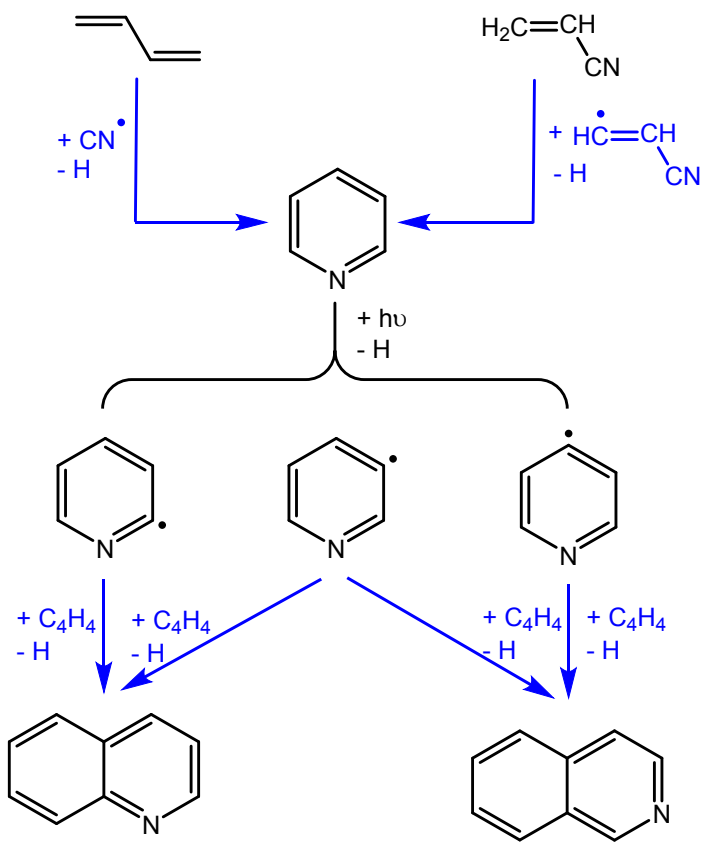


**Figure 6**. Potential pathways leading to the formation of pyridine and subsequently to (iso)quinoline through various mechanisms under low-temperature conditions.